63-3-6

RELATION BETWEEN PHOTOCONDUCTIVITY AND CHEMISORPTION KINETICS FOR STANNIC OXIDE CRYSTALS

by

J. E. Hurt and E. E. Kohnke

Department of Physics
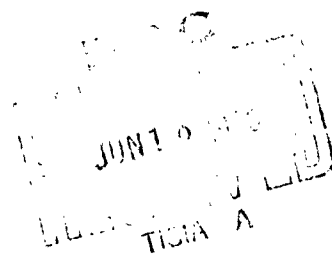
January, 1963
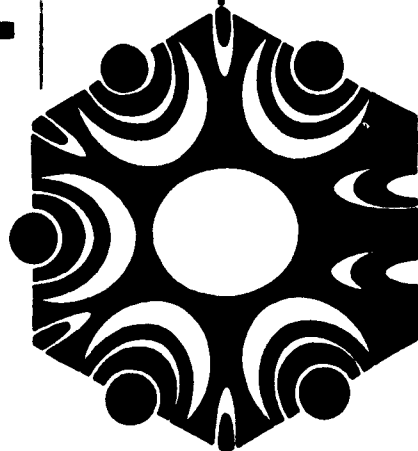
JUN 10

TISIA A

RESEARCH FOUNDATION
OKLAHOMA STATE UNIVERSITY

④ $4.60
⑤ 661900

⑥ RELATION BETWEEN PHOTOCONDUCTIVITY AND CHEMISORPTION KINETICS FOR STANNIC OXIDE CRYSTALS,

⑦ NA
⑧ NA
⑨ Rept. for 1 may 62 - 15 Jan 63,

b) ⑩

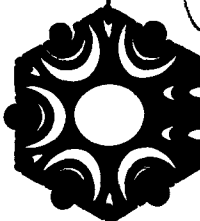J. E. Hurt and E. E. Kohnke,

⑪ 15 Jan 63, ⑫ 44 p.

For the Period
1 May 1962 through 15 January 1963

⑬ NA
⑭ Technical rept. no 2
⑮ Contract Nonr 259501
⑯ Proj NR 015 ≠ 222

17-19 NA

⑳ U.
㉑ NA.

RESEARCH FOUNDATION
OKLAHOMA STATE
UNIVERSITY, STILLWATER

RELATION BETWEEN PHOTOCONDUCTIVITY AND CHEMISORPTION KINETICS

FOR STANNIC OXIDE CRYSTALS*

J. E. HURT AND E. E. KOHNKE

Physics Department, Oklahoma State University, Stillwater, Oklahoma

Abstract — The photoconductive behavior of a number of natural and artificial crystalline specimens of stannic oxide was investigated in various gaseous ambients at pressures ranging from 10^{-2} mm Hg to atmospheric and at temperatures over the interval between 90 K and 355 K. Dependence of photocurrent rise and decay rates on pressure and temperature was also found to be consistent with the predictions of a model relating surface trapping of electrons and Elovich-type chemisorption.

INTRODUCTION

One well known example of a material which crystallizes in the tetragonal rutile structure is provided by stannic oxide, SnO_2. A recent study[1] has utilized results obtained on natural specimens cut from cassiterite crystals in a survey of bulk electrical and optical properties of this substance. Comparison with corresponding properties of the most intensively studied compound in the structural group, TiO_2[2, 3, 4], identified basic differences in the electrical conduction behavior and basic similarities in the optical transmission characteristics which exist between the two. During the course of the investigation many of the stannic oxide samples were found to exhibit photoconductivity characterized by sensitivity to light in the ultra-violet region of the spectrum and by slow rates of photocurrent rise and decay[5], in general agreement with the results of earlier measurements on thin polycrystalline films[6, 7].

The present report has as its purpose a description of these "slow" photoconductive responses which have now been observed in both natural and artificial crystalline specimens and an emphasis on their correlation with oxygen chemisorption kinetics.

The photoconductivity of single crystals of <u>titanium dioxide</u> has been investigated by CRONEMEYER[2], but work linking photoconductivity with chemisorption processes is limited to pressed powder samples. KENNEDY <u>et al</u>.[8] have associated a portion of the photoconductivity characterized by slow rise and decay with the chemisorption of oxygen and nitric oxide. SANDLER[9], also working with powder samples, has found as a result of a study of the ortho-para conversion of hydrogen

2

on diamagnetic surfaces that oxygen adsorbed on titanium dioxide is molecular at 90°K with dissociation occurring at higher temperatures.

Of related interest are studies using oxides of other crystal structures, particularly zinc oxide[10, 11], an n-type broad band semiconductor of hexagonal structure. In this oxide, as well as in both yellow polycrystalline[12] and orthorhombic[13] structures of lead monoxide, photoconductivity has been found to be a surface effect sensitive to the composition of the ambient atmosphere. One photoconduction mechanism proposed for monocrystalline zinc oxide combines a photo-desorption of adsorbed oxygen ions and a photolysis of lattice oxygen ions at the surface[10]. MEDVED[11] has published chemisorption and photoconduction kinetics for sintered samples of zinc oxide and the applicability of his treatment to the surface-sensitive photoconductivity of stannic oxide crystals will provide a basis for much of the following discussion.

SAMPLES

General characteristics of the natural stannic oxide specimens employed in this investigation have been described elsewhere[1]. They were typically transparent, several mm in length and width and fractions of a mm thick, and exhibited n-type room temperature conductivities in the neighborhood of 10^{-4} ohm^{-1} cm^{-1}. After cutting with a diamond saw the broad faces were polished to microscopic smoothness by successive lappings on #320 SiC paper, on a wet glass plate using centriforce abrasive M304 and on white blotting paper impregnated with Linde "A" polishing compound.

3

The artificial samples were grown in this laboratory from a solu-
tion of stannic oxide in cuprous oxide at temperatures near 1200°C. In
form they were needles of rectangular cross section, usually very nearly
square, having lengths between 2 and 4 mm and other dimensions between
0.05 and 0.15 mm. Polarizing microscope studies of several of these
needles indicated that the optic axis lies along their length. Surfaces
were left as they came from the cuprous oxide matrix except for cleaning
and were in general very smooth, showing only microscopic growth patterns.
Typically colorless and transparent, they had a conductivity at room
temperature in the 10^{-6} to 10^{-7} ohm^{-1} cm^{-1} range. Because of their
dimensions, no optical measurements have been carried out on these
samples, but their rutile-type crystal structure has been established
from x-ray diffraction patterns.

More detailed descriptions of individual samples will be included
where applicable in the following paragraphs.

EXPERIMENTAL APPARATUS

The experimental work was carried out in a vacuum system equipped
with a four stage oil diffusion pump. Two sample holders were con-
structed for use with the vacuum system: one, a four-electrode vycor
attachment in the form of a tube 2.2 cm in inside diameter by 19 cm
long, was used for room temperature measurements of the effect of the
ambient on conductivity and photoconductivity; the other, a two-electrode,
two-compartment device of brass and stainless steel provided for the
measurement of photoconductivity in various ambients over a range of
temperatures. The two compartments of the latter sample holder were
a cylindrical coolant chamber having a volume of 120 cm^3 and a

rectangular sample chamber having a volume of 300 cm^3 with an outlet to the vacuum system. Light entered the latter chamber through a quartz window.

In the second sample holder temperatures could be varied from liquid nitrogen temperature to temperatures exceeding 100°C. The particular temperature was determined by the fluid in the "coolant" chamber. A heating coil in water or paraffin oil was used to raise the temperature above room temperature. Temperatures were measured with a copper-constantan thermocouple.

Gaseous ambients other than air were fed into the system from cylinders, following evacuation and sweeping to minimize partial pressures of unwanted gases. A calcium chloride drying tube was attached to the input of the system to remove water vapor. Provision was also made for the addition of water vapor. Pressures were measured by a cold-cathode ionization gauge, a McLeod gauge, or a mercury column manometer.

All light sources used were mercury arc lamps with strong lines in the ultraviolet region of the spectrum. The full spectral output was used in all measurements except the spectral sensitivity determinations, in which a Bausch & Lomb monochromator was employed. Total intensities incident on the samples were in the neighborhood of 10^{-4} watts/cm^2 as a rule.

WAVELENGTH DEPENDENCE OF PHOTOCONDUCTIVITY

The relative responses of the samples used were tested at wavelengths of the strong mercury lines in the near ultraviolet. For the untreated artificial samples it was evident that the photoconduction

edge lies between 313 and 334 mμ or between 3.7 and 4.0 eV. The smaller

and slower responses observed in natural samples provided considerably

less wavelength resolution of the edge but showed no basic disagree-

ment with these figures. Since a value for the optical energy gap,

$E_G \geq 3.54eV$, has already been reported[1] with absorption coefficients

reaching values greater than 10^2 cm^{-1} at shorter wavelengths, light of

sufficient photon energy to induce a photoconductive response is absorbed

in a very thin surface layer of the sample material.

The response maximum observed at 3.44 eV in a previous natural

sample[5] was found to be associated with an indium-rich surface layer.

Upon removal of a thickness of 0.037 mm from the surface, the spectral

response showed the same character as that of the above specimens.

Diffusion of additional indium gave a return to the original pattern.

Confirmation of the increased relative response near 3.44 eV upon indium

diffusion was obtained from other natural specimens. This phenomenon

is under additional investigation in connection with a theoretical

study of possible complexities in the conduction band structure.

EFFECT OF AMBIENT ON PHOTOCONDUCTIVITY

1. Natural samples

Typical curves showing the slow rise and decay of photoconductivity

at room temperature are given in Figs. 1 and 2. The rise curves have

been plotted with time the abscissa and the ratio of total current to

dark current the ordinate. All currents have been corrected for resist-

ances in series with the photoconducting sample. Decay curves have also

been plotted with time the abscissa, but with the ordinate being the

fraction of decay. The symbol i represents the time-varying total

6

current in the sample with i_0 being the dark current and i_{max} the current at the instant illumination ceased.

The two rise and decay curves shown were obtained under equal illumination intensities using Sample IV, a slightly colored sample 0.9 mm thick and having a dark conductivity near 10^{-4} ohm^{-1} cm^{-1}. The decay curves in Fig. 2 correspond to the rise curves in Fig. 1. These clearly illustrate the influence of oxygen on the slow photoconductivity in stannic oxide, suggesting that much, if not all, of the photoconductivity observed in these specimens can be traced to surface phenomena involving oxygen ions. That these decays have a logarithmic character is shown in Fig. 3 where the same data have been replotted with time varying logarithmically.

Further evidence for the importance of ambient oxygen in the slow photoconduction process is presented in Fig. 4 which shows the results of altering the ambient during decay. Sample XVII, with which these curves were obtained, is a colorless sample of moderately low conductivity, similar to Sample IV, but only 0.6 mm thick. The decay shown in Fig. 4 followed a nine-hour exposure in a vacuum of 10^{-7} mm Hg, in which the photocurrent was driven to saturation. The vacuum was maintained during the first thirty minutes of the decay, at the end of which period the vacuum system was opened to an oxygen reservoir and allowed to fill to a pressure of one atmosphere. The influx of oxygen caused an abrupt change in the rate of decay. Results observed in specimens which had undergone only short exposures to illumination were of the same character.

As expected, the nature of the changes was reversed when the ambient was changed during the photocurrent rise under illumination. A decrease in pressure manifested itself in an increased rise rate. On the other

7

hand, the influx of oxygen to a sample being illuminated in vacuum would bring about an immediate decay of an appreciable fraction of the photocurrent followed by a resumption of the rise at a reduced rate.

No corresponding effects were observed using helium or nitrogen. Substitution of wet oxygen for dry oxygen in the experiments provided no significant changes from the results described above. At the upper end of the pressure range, effects due to the presence of oxygen saturated at a partial pressure not exceeding 150 mm Hg while no lower pressure limit (within the experimental range down to 10^{-7} mm Hg) was found below which the importance of the presence of oxygen vanished.

Attempts made at room temperature to detect a dependence of either dark conductivity or contact potential on the gaseous ambient consistently yielded negative results. Air, oxygen, helium and vacua of 10^{-6} mm Hg or less were used. The conductivity was measured potentiometrically and the contact potential by the Kelvin method. Changes in the values of both quantities were sought both statically following ambient change and during dynamic changes. In neither case was there any perceptible effect.

2. Artificial samples

The general characteristics of the photoconductive responses in the artificial samples differ rather markedly from those observed with the natural samples. At room temperature, the photocurrent rise in the artificial samples is quite rapid, the photocurrent reaching saturation within fifteen seconds. The decay is even more rapid, going to completion in 0.01 sec or less. The low conductivity of these samples (in the range between 10^{-7} ohm^{-1} and 10^{-6} ohm^{-1}- cm^{-1}) and their needle-like shape tend to give individual specimens resistances up to 10^{10} ohms.

Consequently, measured dark currents were very low, often 10^{-2} μa or less. However, photocurrents of several μa resulted from ultraviolet illumination of the same type and intensity as that used in work on the natural samples, giving values of i_{max}/i_0 two to three orders of magnitude greater than those measured for natural samples. A typical rise and decay curve for an artificial sample is shown in Fig. 5.

In attempts to detect a dependence of the photoresponse of these samples on the ambient, the responses of several specimens were compared in air, oxygen, and vacuum. No effect was seen at room temperature with oxygen pressures ranging from 740 mm Hg to 5×10^{-8} mm Hg.

The surfaces of two of the artificial samples were roughened to a microscopically frosty appearance using a 600 mesh alumina abrasive. After a thorough cleaning, further measurements of their conductivity and photoconductivity were made. In both samples the end-to-end resistance was reduced to less than 10^7 ohms, indicating that the surface layer removed had played an appreciable role in determining the resistance of the specimens. A computed bulk conductivity of 10^{-4} to 10^{-3} ohm^{-1}- cm^{-1} made these samples comparable with the natural samples. They were also found to more closely resemble the natural specimens in photoresponse, including slow rise and decay and values of i_{max}/i_0 not greatly exceeding unity. The results of tests in various ambients are given in Table I. All exposures in the tabulated series were of one minute's duration, and no change in illumination was made either in the series of experiments involving Sample GII or in that involving Sample GXXII.

The photocurrent decay in artificial samples on which the surfaces had <u>not</u> been roughened was found to be slowed by lowering the temperature of the sample. At temperatures below 200°K the decay was sufficiently

slow to allow measurement of the effect of changing the ambient during
decay. Several trials with representative specimens showed no evidence
of an increase in the decay rate coincident with the entry of oxygen into
the system as was observed with natural samples. In the latter, the effect
of lowering the temperature was only to reduce the dependence of decay
rate upon oxygen pressure without eliminating it entirely, even near
$90^{o}K$. The interpretation of this result will be discussed in detail in
a later section of the paper.

<div align="center">EFFECT OF TEMPERATURE ON PHOTOCONDUCTIVITY</div>

1. <u>Natural samples</u>

   The characteristically observed effect of temperature on the loga-
rithmic decay rates is illustrated in Fig. 6 where results obtained over
a wide range of temperatures with representative Sample IV are plotted.
All curves shown followed one-minute exposures. Whether exposures were
made at atmospheric or reduced pressures the general logarithmic character
of the decays was not altered over the temperature range indicated, the
slopes of the decay curves showed little change between $100^{o}K$ and room
temperature, and there was a tendency for the slopes to increase above
the latter temperature. This effect was particularly pronounced in the
data of Fig. 6.

   It was also noted that at low temperatures the initial rate of
photocurrent decay was dependent upon the duration of the exposure.
Two relatively short exposures, one of five times the duration of the
other, are shown in Fig. 7. Both are for Sample IV in vacuum, the one-
minute exposure being at $110^{o}K$ and the five-minute exposure at $88^{o}K$
under a higher illumination intensity. Additional evidence of this
effect is given in Table II.

<div align="center">10</div>

Table II further shows not only that decay rates were slowed by lengthening the period of illumination, but that mechanical roughening of the broad faces of Sample XIIIA also acted to retard decay at low temperatures.

The logarithmic decay illustrated in Fig. 6 is not linear during the first seconds of the decay. This deviation from linearity was commonplace except at low temperatures. If a constant is added to the time coordinate at each point--in effect shifting the entire curve to the right--the curve becomes linear throughout. The additive factor required must be determined individually for each curve and will be designated as a "decay-time constant", t_d. The measured values of t_d and the decay slopes of the linearized logarithmic decay curves for Sample IV following identical one-minute exposures in air at atmospheric pressure increased from 2.0 to 6.0 sec and 0.11 to 0.31 respectively in the temperature range between 270 and 350°K.

Another effect noted in the logarithmic decay curves was the drop below linearity beginning before completion of the decay. In some cases this occurred with the decay considerably less than fifty per cent complete. Reference to the oxygen decay curve of Fig. 3 provides an example. It became apparent that there was a relationship between the time required for this effect to become noticeable and the illumination period. This is best represented, however, as a systematic dependence on the ratio $\Delta i/i_{max}$, where $\Delta i = i_{max} - i(t)$ is now understood to represent the decrease in current up to the time of onset of sublinearity. The dependence is illustrated in Table III. Except in Sample IV, the room temperature value of $\Delta i/i_{max}$ lies between 0.1 and 0.2. Also it can be seen that for equal exposure times in both Sample III and Sample IV there is a definite decrease in $\Delta i/i_{max}$ as temperature increases.

2. Artificial samples

The response of artificial Sample GI was measured over the temperature range between 122°K and room temperature. While the character of the rise was not seen to change appreciably, a considerable decrease in the decay rate at low temperatures was noted. This decrease was perceptible at 239°K, the decay taking about five seconds to go to completion at that temperature. At 250°K the decay was complete within less than one second, essentially the sharp drop shown in Fig. 5. Figure 8 shows the logarithmic decay curves for Sample GI at several reduced temperatures. While none are linear, it should be noted that $(i_{max}-i)/(i_{max}-i_o)$, which is equal to $\Delta i/i_{max}$ to within one per cent, is large for all data points.

Rise curves at low temperatures saturated quickly as did room temperature rise curves. Under the same illumination, the saturation photocurrent measured for Sample GI was 0.75 μa at 122°K and 0.83 μa at 298°K, the applied voltage being 40 V in both cases.

DISCUSSION

1. General description of the model

The tenor of the results given in the previous sections suggests that a model recently used by MEDVED[11] to describe a correlation between photoconductivity and chemisorption kinetics in sintered samples of zinc oxide may have applicability to stannic oxide. As details are available elsewhere, only the basic relationships will be presented here.

Briefly, one visualizes the slow photoconduction mechanism in the following way. A depletion-type space charge layer exists at the surface of the stannic oxide crystal due to the presence of chemisorbed oxygen ions. An ultraviolet photon absorbed near the surface creates a

12

hole-electron pair. The hole is drawn rapidly by coulombic attraction
to the surface where it neutralizes an adsorbed negative oxygen ion,
releasing it to be held by physical adsorption forces. The removal of
holes from the valence band leaves an excess of conduction electrons to
act as photocurrent carriers. If the source of excitation is withdrawn,
the photocurrent decays as recombination takes place at physically
adsorbed oxygen sites on the surface with the transport of electrons
across the surface potential barrier acting as the rate-determining pro-
cess. On the other hand, under continued illumination a quasi-equilibrium
state will be attained with ultimate saturation of the photocurrent.

Combined with simplifying assumptions that the direct contribution
of holes to the photocurrent is negligible, the fractional change in
carrier density is large compared with the fractional change in chemi-
sorbate density, processes governing physical adsorption act rapidly in
comparison with the basic rate-limiting process, and chemisorption binding
energies are large compared to thermal energies involved, the model pre-
dicts a chemisorbate density rate increase (photocurrent decay process
following removal of illumination) of the empirical Elovich form

$$\frac{dq}{dt} = a \exp[-bq] \tag{1}$$

where $a = svq_p n$ and $b = e^2 d/2KkT$.

For identification of symbols:

    q = surface density of chemisorbed species

    s = capture cross section of physically adsorbed species for an
        electron on the surface

    q_p = surface density of physically adsorbed species

    v = average thermal velocity of electrons

13

n = volume density of electrons

e = electronic charge

d = space charge layer thickness

K = static dielectric permittivity of surface layer

k = Boltzmann constant.

Use has been made of a Richardson-Dushman thermionic emission equation form for the rate of barrier penetration by electrons and of the Poisson relation to obtain a space charge layer potential difference based on a linearized electric field.

For the illumination period (photocurrent rise process), equation (1) must have added to it a photodesorption term:

$$\frac{dq}{d\tau} = a \ exp[-bq] - L \tag{2}$$

where use is made of τ rather than t to emphasize the different time frame involved. Saturation of the photocurrent rise will occur when the two terms reach a balance.

To convert these equations to the corresponding rate equations for carrier density one further assumes a one-to-one correspondence between the number of added conduction electrons and the number of chemically desorbed oxygen ions. For the decay process this leads to

$$\Delta q \equiv (q-q_f) = x_0 (n_f - n) \equiv x_0 \Delta n \tag{3}$$

where x_0 is a geometrical factor giving the ratio of the volume of the crystal under consideration to the area illuminated. The subscript f identifies the densities at the time illumination ceased (a maximum for n). The nonsubscript terms are the densities at the instant of the measurement.

Substitution for q and integration leads to the decay curve expression

14

$$\Delta n = \frac{1}{B} \ln(t/t_d + 1) \tag{4}$$

where $B = bx_0$ and $t_d^{-1} = bn_f svq_p \exp[-bq_f]$. This expression is an approximate solution, correct to first order for $\Delta n/n_f$ small. It will be noted that it predicts a carrier density decay which is linear with $\ln(t+t_d)$. A direct comparison can be made with current changes in ratio form on the assumption that carrier mobility remains constant during the experiment and thus current changes are dependent entirely upon carrier density changes. As t increases to values at which $\Delta n/n_f$ becomes appreciable, second order effects cause the relationship between Δn and $\ln(t+t_d)$ to take on a sublinear character.

A similar treatment can be applied to the photocurrent rise time problem leading to an expression for the carrier density increase

$$\Delta n_e = -\frac{1}{B} \ln[A_1/L + (1-A_1/L)\exp(-bL\tau)] \tag{5}$$

where the subscript e refers to the densities in the dark, i.e., $\Delta n_e \equiv (n-n_e)$, and $A_1 = a \exp[-bq_e]$. This equation is also an approximation, valid only for small carrier density changes leaving A_1 essentially constant and assuming a constant photodesorption rate L. Additionally, any appreciable fractional change in q will destroy the constancy of b.

The relative simplicity of equation (4) makes data obtained in photocurrent decay measurements most useful for interpretation as will be shown in succeeding sections.

2. <u>Qualitative agreement with predicted results</u>

The predicted logarithmic decay rate is quite strikingly illustrated in Figs. 3 and 6 for times $t > t_d$. Values of t_d can be determined empirically and have values of several seconds as previously described. Furthermore, the prediction of sublinear decay rates at times when

$\Delta n/n_f$ becomes appreciable is borne out by the data given in Table III.

A Langmuir isotherm dependence of q_p on pressure leads to a prediction by equation (1) of an enhancement of the fractional decay rate with increasing pressure following cessation of illumination. Similarly, equation (2) predicts an enhancement of the rise rate with decreasing pressure under constant illumination. The over-all importance of pressure in determining rise rates will be less than the importance of pressure in determining decay rates because two competing process are involved. This is in accord with the observations made on natural and roughened artificial specimens. As can be seen, however, the pressure dependence of decay rates is quite small for these samples and nonexistent for artificial crystals which have not been roughened, necessitating the introduction of an additional feature into the basic model.

In both artificial and natural specimens the decay rate decreases under constant pressure with decrease in temperature as would be expected from the inverse temperature dependence of the factor b. At temperatures in the range of $160^{\circ}K$ or below the fractional decay occurring in the first few seconds goes through a minimum which also calls for an alteration of the original model.

3. Calculation of significant parameters

The use of crystals for which Hall effect determinations of carrier densities are available makes it possible to estimate the numerical value of several significant parameters included in the model.

One typical example is provided using the magnitude of B determined from logarithmic decays following one-minute exposures of natural Sample IV at room temperature and atmospheric pressure. The value of the

16

carrier density in the dark coupled with the current increase provides a figure for the density change, Δn, for the entire rise. A maximum value for x_o can be determined from geometry. Appropriate magnitudes for these quantities are $B = 1 \times 10^{-12}$ cm^3, $n = 8 \times 10^{12}$ cm^{-3} and $x_o = 0.13$ cm respectively. Using the expression previously given for b and a static dielectric constant[14] of 24, one obtains a space charge layer thickness of 5×10^{-6} cm as a representative end-of-illumination value. The quantity $C_{\mathbf{a}} = 2K/d$ may be defined as the surface layer capacitance/area and is calculated to be 0.83 $\mu f/cm^2$. From the basic assumption that $\Delta q = x_o \Delta n$, the resulting maximum chemisorbate density change is 1×10^{12} cm^{-2}.

Actual magnitudes of the chemisorbate density are arrived at in an indirect manner. By using exposures of several hours, Sample IV was driven to photoconductive saturation in two ambients which had an oxygen partial pressure ratio of 5×10^{-8}. A comparison of the initial decay rates following saturation gave a ratio of 6.5, decay being more rapid for the higher pressure observation. Assuming that the adsorption rates immediately preceding and immediately following termination of illumination are the same and that s and v are substantially the same for the two pressure conditions, it follows that

$$\frac{\left[\frac{dq}{dt}\right]_{t=o}^{(L)}}{\left[\frac{dq}{dt}\right]_{t=o}^{(H)}} \equiv \frac{\left[\frac{d(\Delta n)}{dt}\right]_{t=o}^{(L)}}{\left[\frac{d(\Delta n)}{dt}\right]_{t=o}^{(H)}}$$

$$= \left[\frac{q_p(L)}{q_p(H)}\right] \frac{n_s(L)}{n_s(H)} \exp\left\{B(L)\left[\Delta n_s(L) - \frac{q_s}{x_o}\right] - B(H)\left[\Delta n_s(H) - \frac{q_s}{x_o}\right]\right\} \quad (6)$$

where (L) and (H) identify quantities measured respectively in the low pressure and high pressure experiments and the subscript s indicates photocurrent saturation values.

Using observed magnitudes in the above relation leads to a minimum value for the physical adsorbate density ratio of 1×10^{-5} under the restriction that $q_s/x_o > \Delta n_s(L)$. This less-than-linear dependence of physical adsorbate density on pressure will be discussed in the next section.

On the other hand, placing the restriction that the physical adsorbate density ratio should not depend inversely on the pressure ratio gives the maximum chemisorbate density in the dark of 7.9×10^{12} cm^{-2}. The exponential character of the relationship furthermore allows only about 50% difference between the minimum and maximum values of q_s/x_o. These results give an upper limit of less than 1% of a monolayer chemisorbate coverage and severely reduce the validity of the $\Delta q/q \ll \Delta n/n$ assumption since these two quantities at best are of the same order of magnitude. Consequently, the use of a constant b is well-grounded only for relatively short portions of the decay which is another factor hastening the time of onset of sublinearity in the logarithmic decay curves.

The same sort of limiting procedure allows a rough estimate for the dark surface barrier height ($E_s = kTb_s q_s$) of ≈ 1.6 eV and a minimum barrier height decrease of 0.2 eV during a one-minute illumination. It should be noted that the geometrical ratio x_o may be too large by a factor of 3 to 5 due to surface roughness. While the barrier height estimation is independent of this quantity, use of a smaller value will give correspondingly larger values of d and smaller values of C_a and q_s.

4. Additional temperature and pressure dependence considerations

A simple picture of physical adsorption such as that provided by DE BOER[15] leads to an expression of the form

$$q_p = Const. \times PT^{-\frac{1}{2}} \exp[Q/RT] \qquad (7)$$

for the physical adsorbate density on a surface. Here Q is the heat of physical adsorption which is generally found in the range of 3 to 4 k.cal/mole for oxygen on a variety of surfaces. It is evident from the form of equation (1) where a contains the q_p term that at constant temperature the surface barrier energy plays the major role in determining the chemisorption rate and hence the photocurrent decay rate.

On this basis, the rapid decay of photocurrent in artificial samples retaining their original surfaces implies a considerably lower surface barrier than that calculated above for natural samples if the same type of analysis is to be applied. Although current increases of two orders of magnitude were observed under illumination, lower initial carrier densities and a larger surface-to-bulk ratio than existed in natural specimens make these possible to achieve with small chemisorbate density changes and little decrease in the surface barrier. Experimental evidence is provided by the rapid saturation at a current level which is independent of the ambient pressure.

At lower temperatures it is observed that the rate of photocurrent decay decreases. The competition of the two exponential terms in equation (1) thus places a lower limit of about 0.15 eV on the surface barrier height if the surface is uniformly active in the physical adsorption process. Even in this temperature range, however, no dependence of either rise rate or decay rate on pressure is detected.

Inspection of equation (6) reveals that the exponential term reduces to the difference of the final barrier heights in units of kT when photocurrent saturation has been attained under two different pressure conditions. To compensate for eight orders of magnitude pressure change with no difference of initial decay rate would require a barrier height difference of some 3 kT, an unreasonably large fraction of the total barrier in view of previous conditions.

It is therefore proposed that the physical adsorbate density does not vary linearly with pressure as has already been suggested by the calculations of the previous section. The heat of physical adsorption is of the order of 6 kT even at room temperature, making it plausible that oxygen chemically desorbed by the action of light does not immediately come into equilibrium with the ambient atmosphere at reduced temperatures and thus provides a physical adsorbate density in excess of the value predicted by equation (7). In line with this addition to the basic chemisorption model are the reduced pressure dependence of both rise and decay rates at low temperatures in natural as well as in grown specimens and the decrease in initial decay rate with length of exposure illustrated in Fig. 7. The observation of a minimum initial decay rate near $160°K$ suggests that in this temperature range the presence of additional oxygen provided by the action of light but not immediately removed from the surface outweighs in importance the competing exponential terms involving the heat of physical adsorption and the surface barrier height.

To be consistent with this view for short exposures at fixed reduced temperature and pressure, the sum of the two types of adsorbate densities must remain essentially constant and the chemisorbate density must be appreciably larger than the physical adsorbate density.

20

Data from several decay curves for Sample GI have been examined

under these requirements in the region of decay following the initial

fast portion. Using constant $q_o \equiv q_p + q(t)$, equation (1) may be

rewritten as

$$\frac{dq(t)}{dt} = \gamma n_s \left[\frac{n(t)}{n_s}\right]\left[q_o - q(t)\right] \exp\left[-bq(t)\right] \tag{8}$$

where γ is a constant factor. If $q_e \doteq q_o$, equation (8) becomes

$$\frac{dq(t)}{dt} = \gamma n_s (q_e - q_s) \left[\frac{n(t)}{n_s}\right]^2 \exp\left[-bq(t)\right] \tag{9}$$

since $\left[q_e - q(t)\right] / \left[q_e - q_s\right] = n(t)/n_s$.

The results for a typical decay are given in Table IV at a number

of points as time increases. The quantity S is obtained from the photo-

current decrease rate and hence is proportional to the rate of chemi-

sorbate increase $dq(t)/dt$. The quantity F is the fractional photocurrent

remaining or $n(t)/n_s$. The compatibility of the observations with the

two assumptions is evident in the constancy of the S/F^2 ratio as in

this region of the decay there will be only an insignificant change in

the barrier height and hence an essentially constant value for the

exponential term.

CONCLUSIONS

It is apparent from the preceding discussion that a chemisorption

model successfully predicts the gross features of the photoconductive

behavior in both natural and artificial stannic oxide crystals and pro-

vides a reasonable set of values for significant parameters.

Still lacking are a specific knowledge of the ionic character of

the chemisorbed species and a detailed understanding of the nature and

diversity of the different types of adsorption sites present. Independent

21

data on surface potentials as well as energies and densities of trapping states are being sought by field effect methods.

REFERENCES

1. Kohnke E. E., *J. Phys. Chem. Solids* **23**, 1557 (1962).

2. Cronemeyer D. C., *Phys. Rev.* **87**, 876 (1952).

3. Breckenridge R. G. and Hosler W. R., *Phys. Rev.* **91**, 793 (1953).

4. Frederickse H. P. R. and Hosler W. R., *National Bureau of Standards Report* 6585 (1959).

5. Kohnke E. E. and Hurt J. E., *Bull. Amer. phys. Soc.*, Ser. II, **4**, 428 (1959).

6. Andrievskii A. T. and Zhuravlev V. A., *Sov. Phys. Doklady* **1**, 239 (1956).

7. Ishiguro K., Sasaki T., Arai T. and Imai I., *J. phys. Soc. Japan* **13**, 296 (1958).

8. Kennedy D. R., Ritchie M. and MacKenzie J., *Trans. Faraday Soc.* **54**, 119 (1958).

9. Sandler Y. L., *J. phys. Chem.* **58**, 54 (1954).

10. Collins R. J. and Thomas D. G., *Phys. Rev.* **112**, 388 (1958).

11. Medved D. B., *J. Phys. Chem. Solids* **20**, 255 (1961).

12. Izvozchikov V. A., *Sov. Phys. Solid State* **3**, 2344 (1961).

13. Bigelow J. E. and Haq K. E., *J. appl. Phys.* **33**, 2980 (1962).

14. Berberich L. J. and Bell M. E., *J. appl. Phys.* **11**, 681 (1940).

15. De Boer J. H., *The Dynamical Character of Adsorption*, Clarendon Press, Oxford (1953).

TABLE I

EFFECT OF AMBIENT ON PHOTORESPONSE OF ARTIFICIAL
SAMPLES HAVING ROUGHENED SURFACES

Sample	Ambient*	$\frac{i_{max}}{i_o}$	$\frac{i_{max} - i}{i_{max} - i_o}$ (at 30 sec)
GII	Air	1.04	0.51
GII	O_2	1.03	0.52
GII	7.5×10^{-6} mm Hg	1.07	0.35
GXXII	Air	1.10	0.43
GXXII	1×10^{-6} mm Hg	1.14	0.38

*At atmospheric pressure unless specified otherwise.

TABLE II

COMPARISON OF PHOTOCURRENT DECAYS AT LOW TEMPERATURE

Sample	Ambient*	Temperature ($^{\circ}$K)	Exposure time (min)	$\dfrac{i_{max} - i}{i_{max} - i_o}$ (at 30 sec)
XIIIA (rough)	3×10^{-3} mm Hg	94	1.00	0.29
XIIIA (rough)	1×10^{-2} mm Hg	99	0.50	0.44
XIIIA (rough)	3×10^{-3} mm Hg	102	1.00	0.74
XIIIA (rough)	3×10^{-3} mm Hg	109	0.75	0.80
XIIIA (smooth)	3×10^{-3} mm Hg	114	1.00	0.69
IV	3×10^{-3} mm Hg	106	1.00	0.85
IV	1×10^{-4} mm Hg	88	5.00	0.12
IV	Dry O_2	81	5.00	0.20
IV	Dry O_2	95	5.00	0.14
IV	Dry N_2	85	5.00	0.15
IV	He	136	5.00	0.06
IV	He	139	5.00	0.08
IV	He	146	10.00	0.02
IV	He	146	10.00	0.04

*Ambient at atmospheric pressure or the appropriate vapor pressure unless specified otherwise.

TABLE III

PARAMETERS ASSOCIATED WITH THE ONSET OF SUBLINEARITY
IN LOGARITHMIC DECAY CURVES

Sample	Ambient	Temperature (^{O}K)	Exposure time	$\frac{\Delta i}{i_{max}}$	t*
III	Air	270	30 sec	0.29	20-25 sec
III	Air	296	30 sec	0.18	20-25 sec
III	Air	309	30 sec	0.12	20-25 sec
IV	Air	272	1 min	0.13	45-60 sec
IV	Air	280	1 min	0.061	45-60 sec
IV	Air	281	1 min	0.066	45-60 sec
IV	Air	297-298	1 min	0.022	45-60 sec
IV	Air	297	50 min	0.034	90 min
IV	Air	297	500 min**	0.037	85 min
IV	Air	309	1 min	0.015	45-60 sec
IV	Air	317	1 min	0.010	45-60 sec
VIIIB	O_2	297	10 min	0.14	22 sec
VIIIB	Vacuum	297	10 min	0.11	20 sec
XVII	O_2	297	540 min**	0.18	75 min

*t = time of onset of sublinearity, measured from start of decay

**photocurrent reached saturation

TABLE IV

VARIATION OF F AND S FOR SAMPLE GI AT 190°K

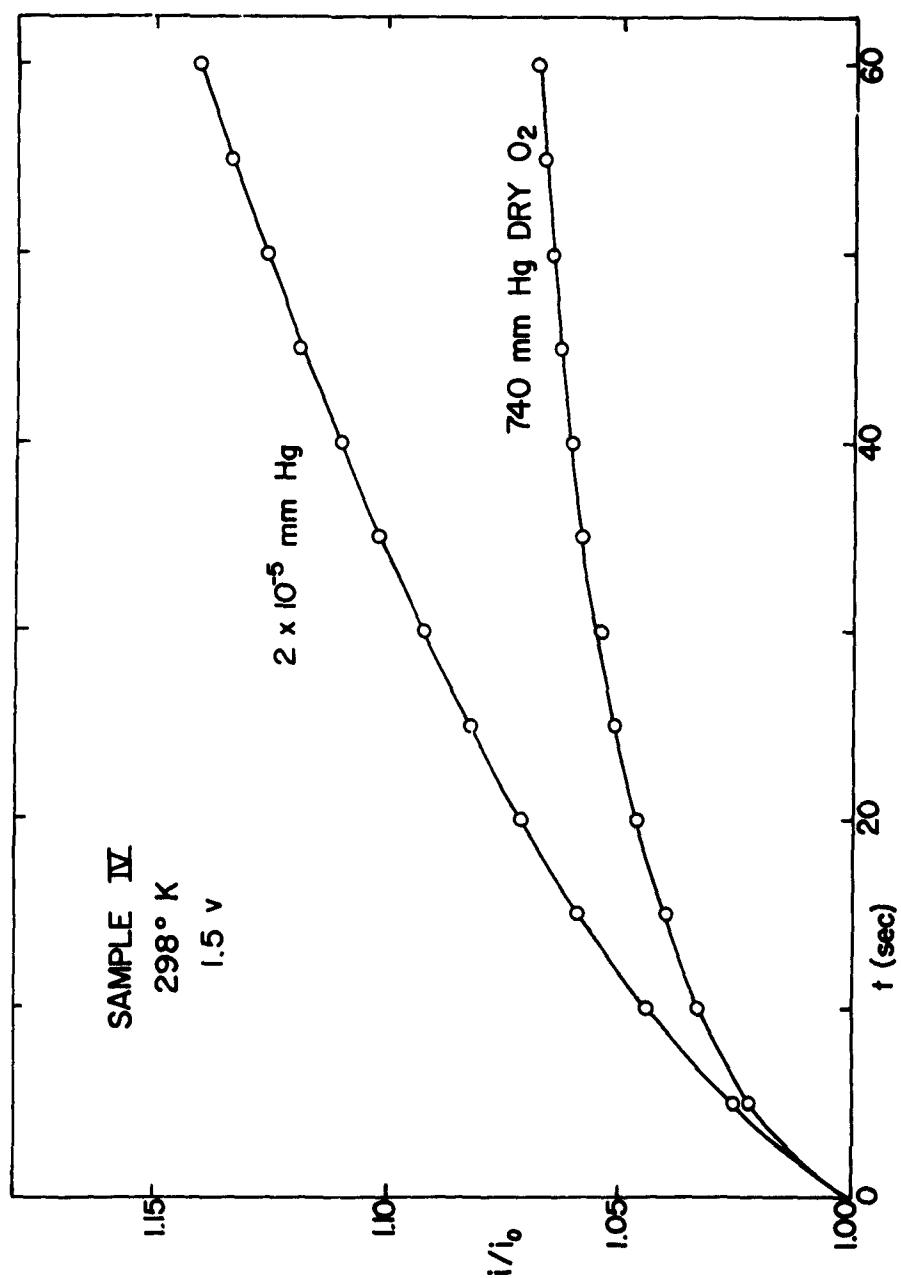| F	S	S/F	ln(S/F)	S/F^2
0.23	1.56	6.8	1.917	29.5
0.20	1.22	6.1	1.808	30.5
0.16	0.70	4.4	1.481	27.5
0.13	0.49	3.8	1.335	29.2
0.10	0.31	3.1	1.131	31.0
0.09	0.21	2.3	0.833	25.6

Figure 1. Typical photocurrent rise curves for a natural sample
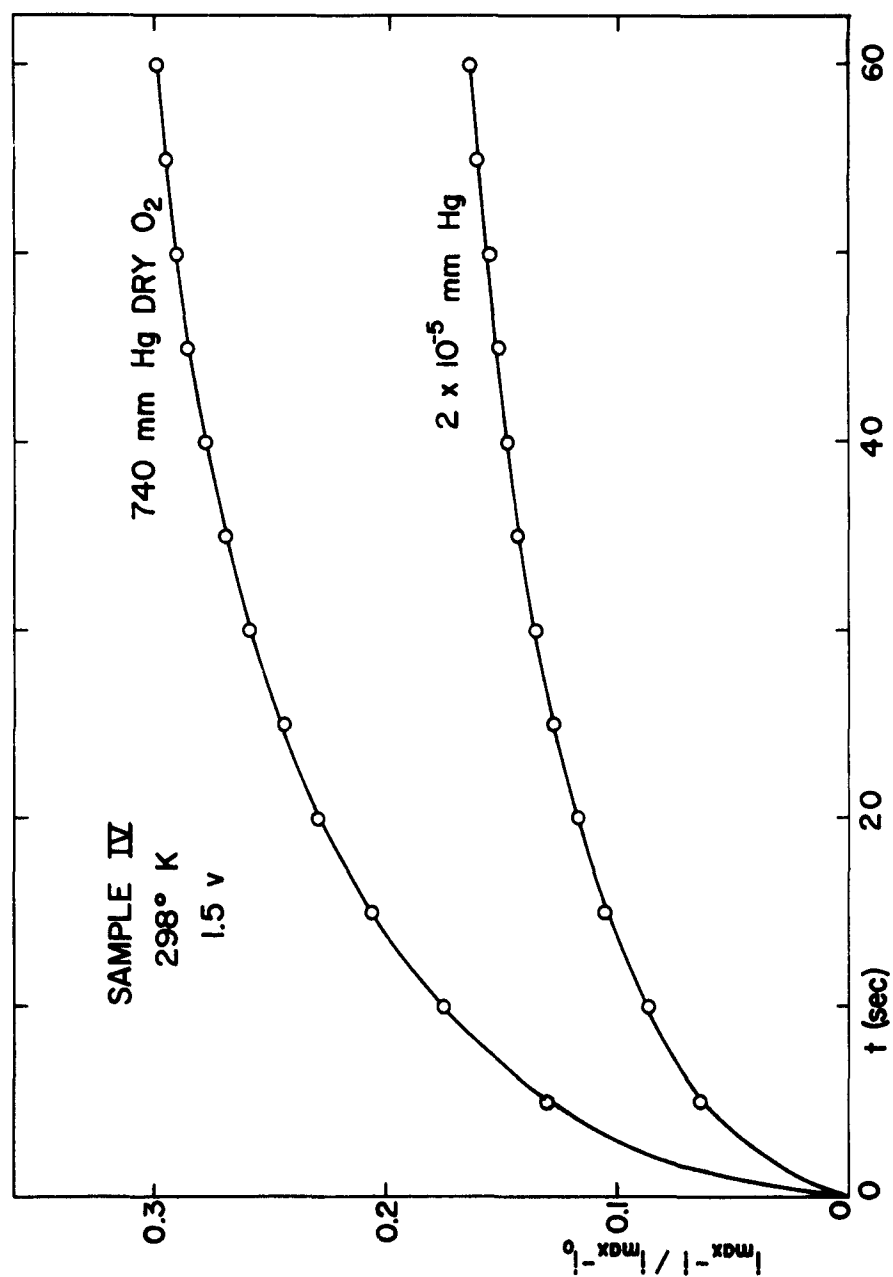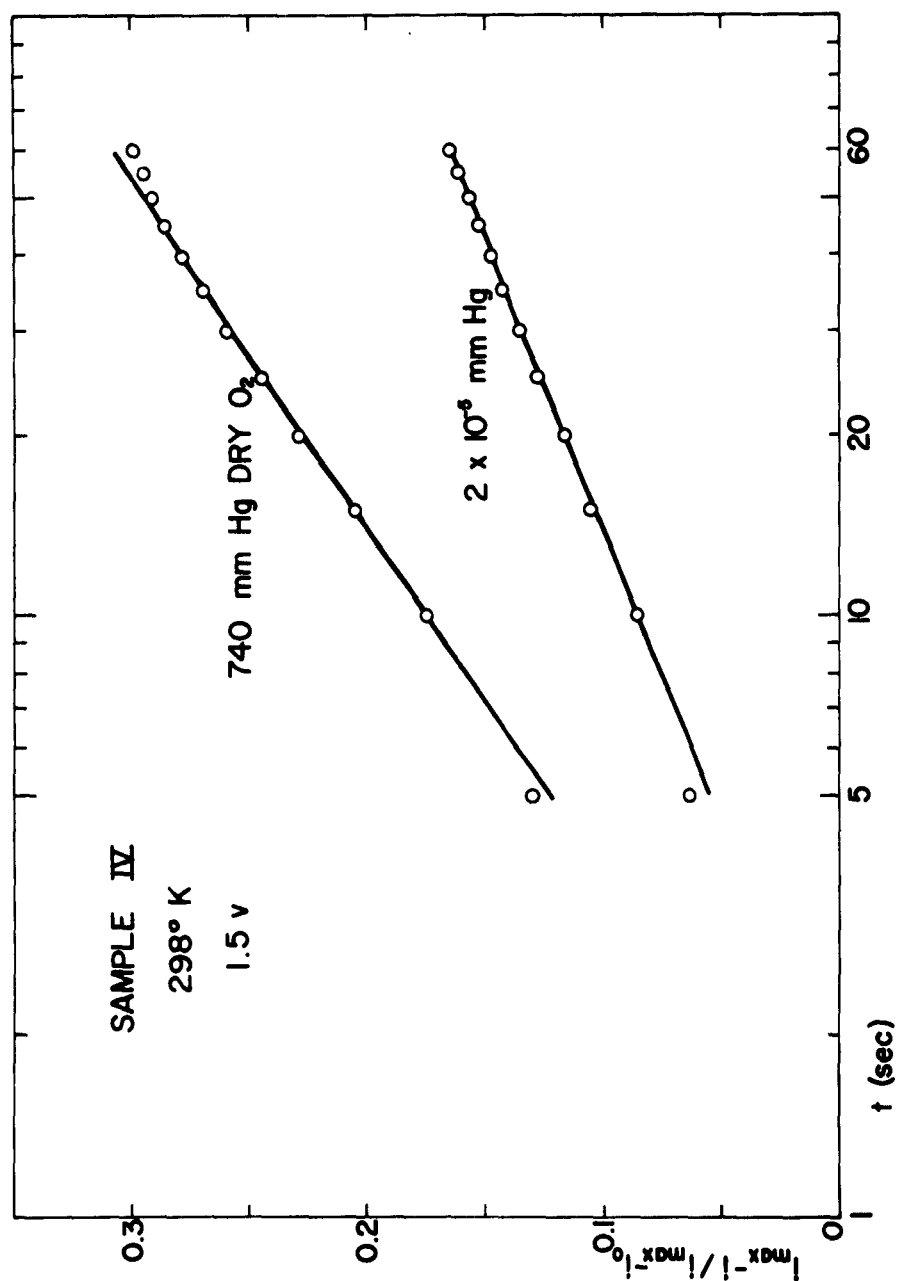
Figure 2. Typical photocurrent decay curves for a natural sample

Figure 3. Logarithmic decay curves for a natural sample
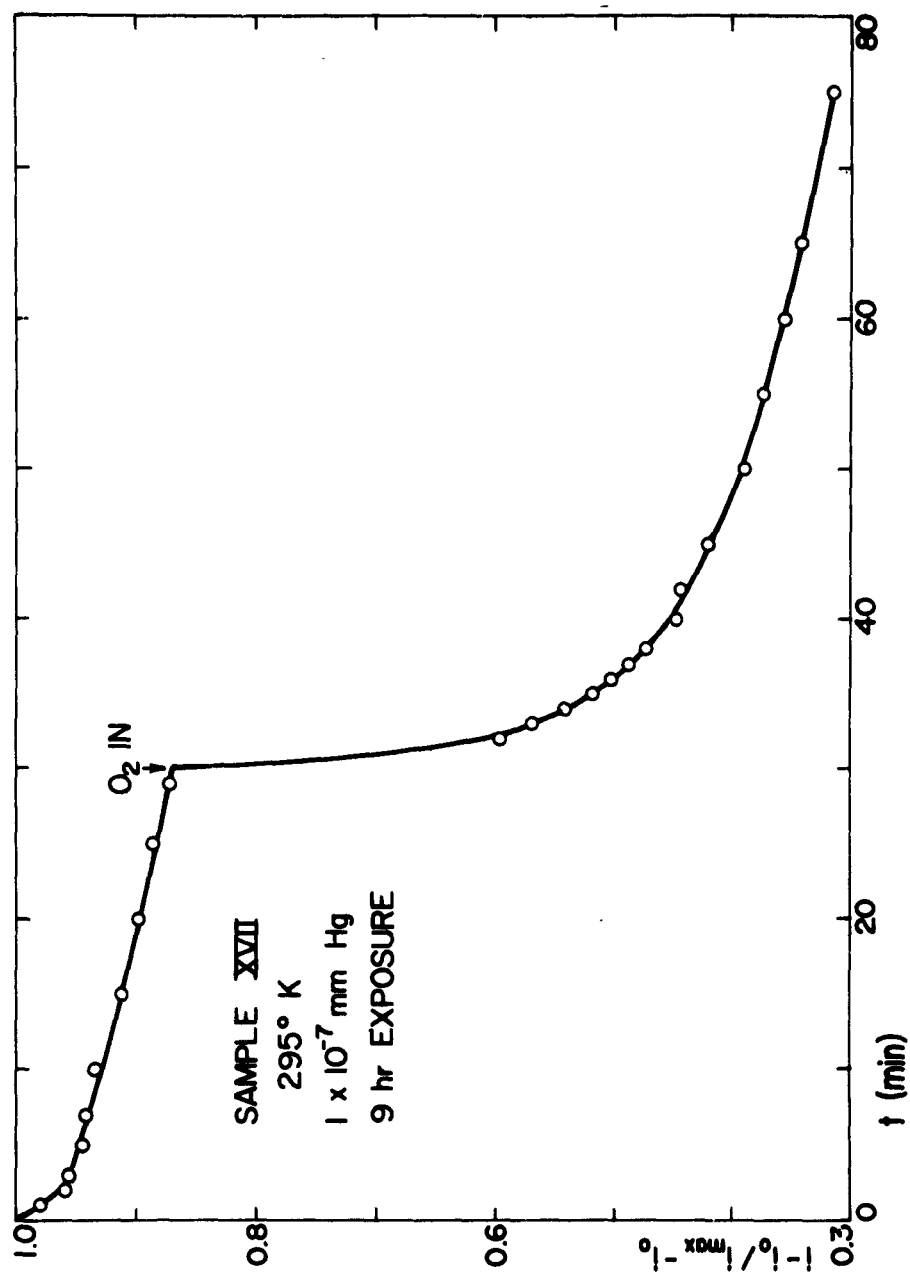
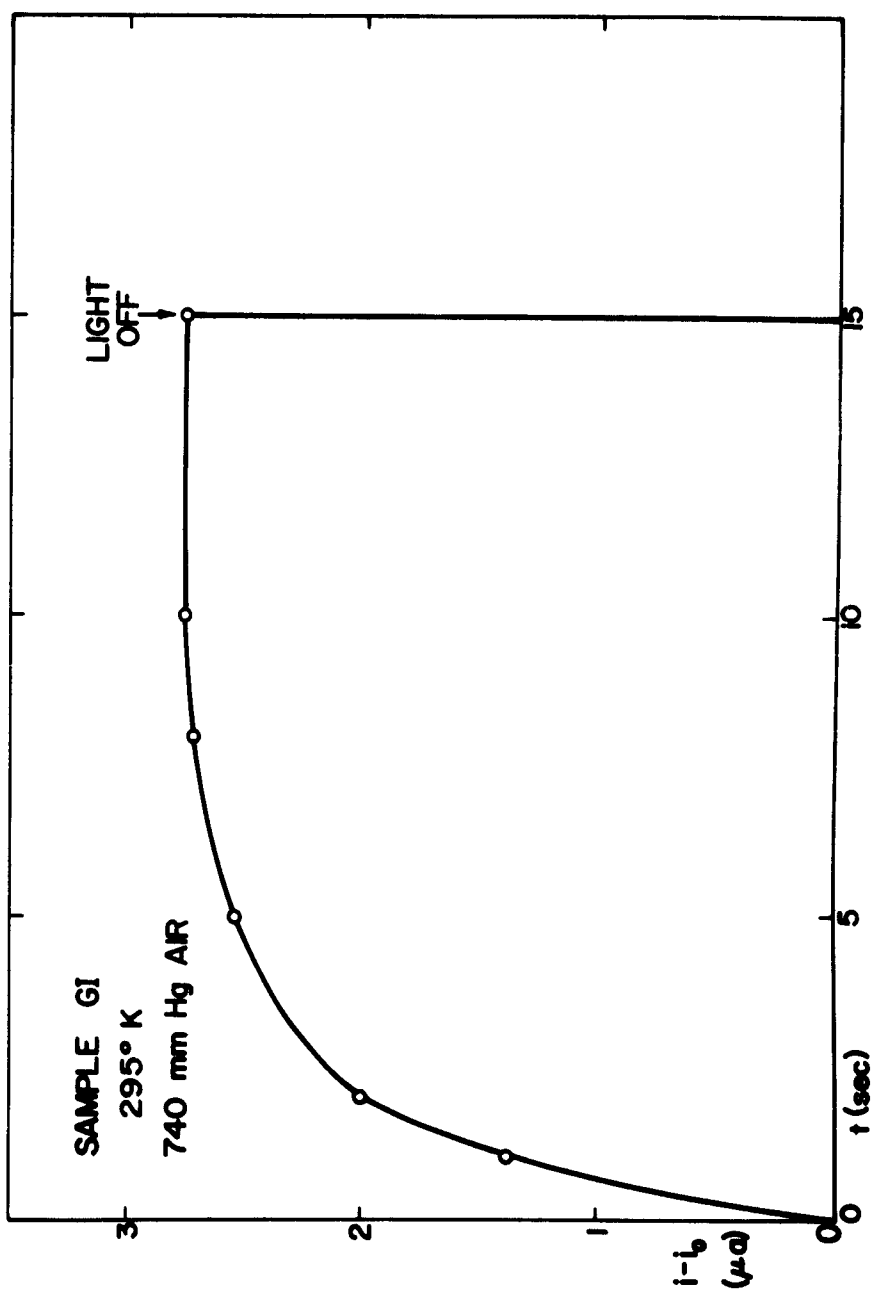Figure 4. Effect of oxygen admission on decay

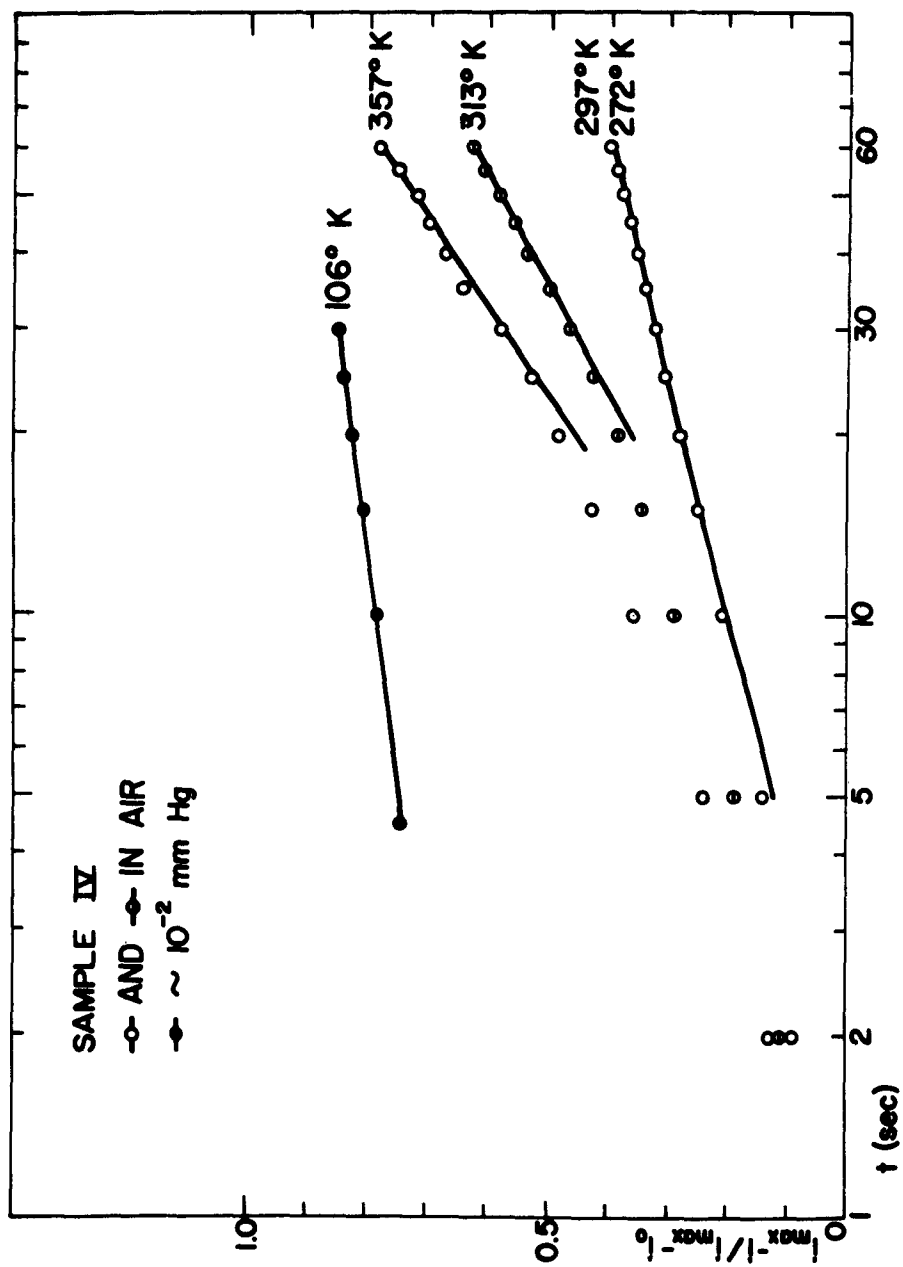Figure 5. Typical rise and decay of photocurrent for an artificial sample

Figure 6. Logarithmic decays for Sample IV at several temperatures
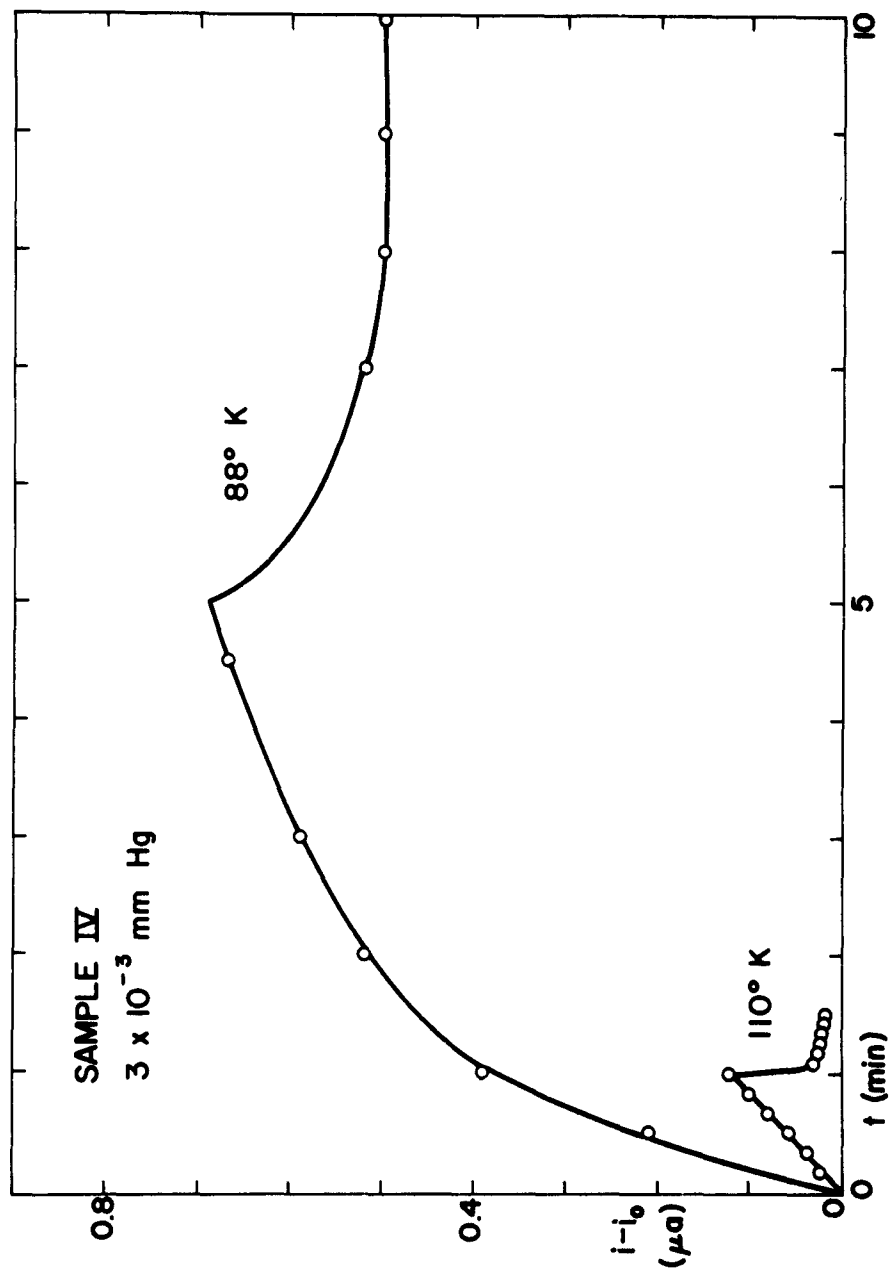
Figure 7. Typical rise and decay curves for a natural sample at low temperature
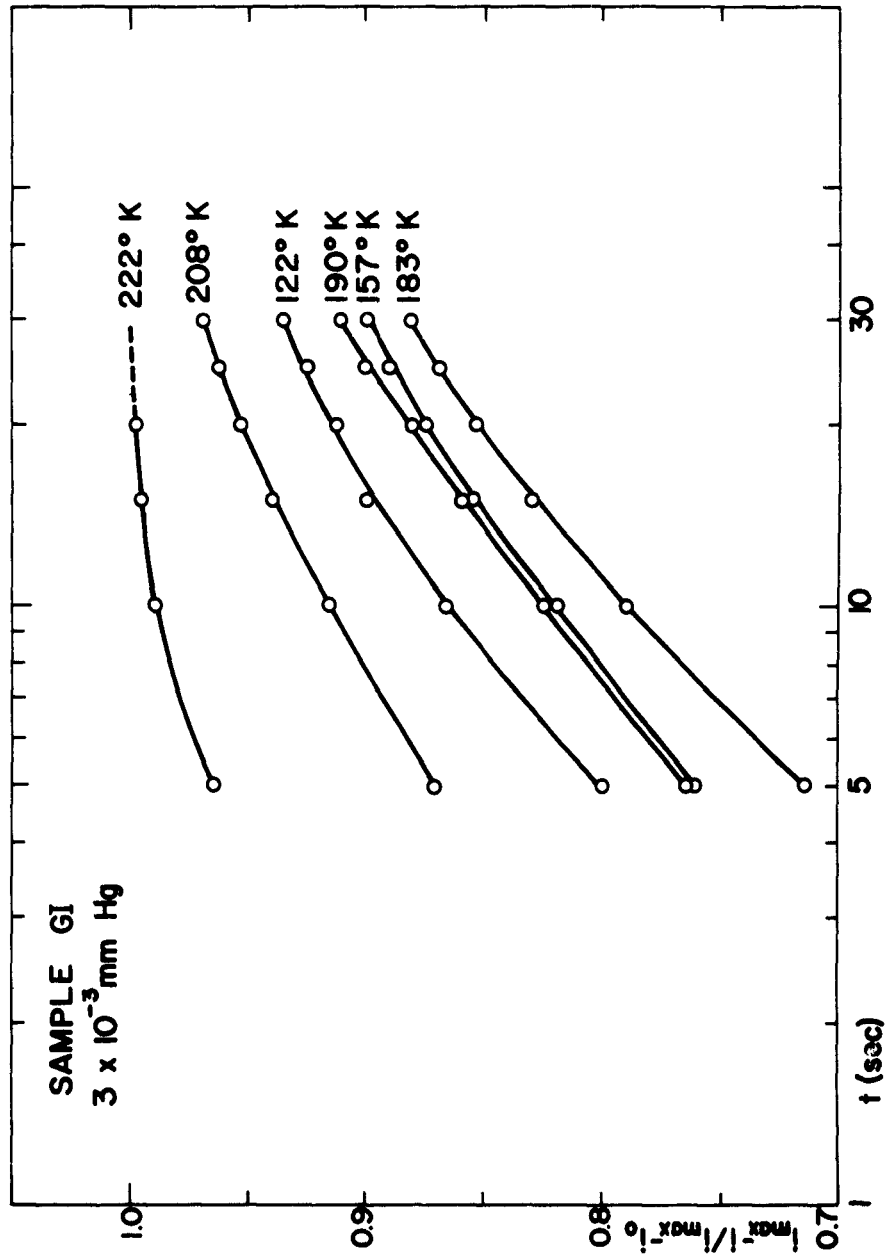
Figure 8. Effect of temperature on photocurrent decay in a typical artificial sample

MATHEMATICAL APPENDIX

This mathematical appendix is presented to supplement the very brief description of the basic chemisorption model given in the main body of the report. The present form has been provided by MEDVED[11] and represents an extension of the work done in recent years by a number of investigators at the University of Pennsylvania who have been studying the relationship between photoconduction and Elovich-type chemisorption in zinc oxide. The essential elements of this treatment follow.

It is first necessary to make the following simplifying assumptions:

1. Holes generated by photon absorption either recombine with conduction electrons or migrate to the surface in a time very short compared to that involved in the basic rate-limiting process, so that the direct contribution of holes to photoconduction is negligible.

2. $\Delta n/n \gg \Delta q/q$, where n is the volume density of conduction electrons and q is the surface concentration of the chemisorbed species.

3. Processes governing physical adsorption act rapidly in comparison with the basic rate-limiting process.

4. $\Delta N = \Delta Q$, where ΔN is the change in the total number of conduction electrons and ΔQ is the change in the total number of chemisorbed oxygen ions.

The rate equation for chemisorption can now be written in the form

$$\frac{dq_c}{dt} = sq_p\eta_e - \zeta q_c - L \qquad (1)$$

where q_c and q_p are surface concentrations of chemisorbed and physically adsorbed oxygen respectively, s is the capture cross section of the physically adsorbed species for an electron on the surface; η_e is the number of conduction electrons penetrating each square centimeter of the surface barrier per second, ζ is the rate of desorption due to thermal excitation, and L is the photodesorption rate term. The barrier penetration process is fundamentally the same as that of thermionic emission, so η_e can be calculated using the Richardson-Dushman equation. Therefore,

$$\eta_e \doteq n\bar{v}(T) \exp[-E(q_c)/kT] \qquad (2)$$

where n is as above, $\bar{v}(T)$ is the averaged thermal velocity of the conduction electrons, $E(q_c)$ is the energy height of the surface barrier, k is Boltzmann's constant, and T is the absolute temperature. With negative charge held at the surface by chemisorbed oxygen ions, the surface barrier should consist of a "depletion layer," i.e., a space charge layer in which the density of conduction electrons is reduced because of electrostatic repulsion from the negatively charged surface. Such a barrier layer is shown schematically in Fig. 1A, with the barrier height $E(q_c)$ and the "chemisorption binding energy" E_c indicated.
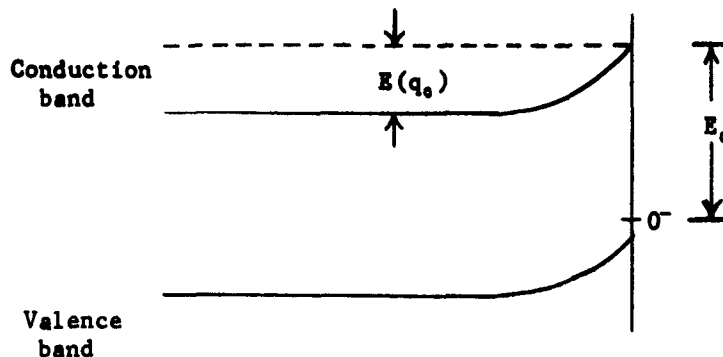
Figure 1A. Surface Energy Level Diagram

E_o is much larger than $E(q_c)$ for all values of q_c. Binding energies for chemisorption are usually in the range between one and three electron volts. Since E_o can be considered to be much greater than any thermal energies to be dealt with here, the second term in Equation 1 is negligible. Thermal energies of interest will have an upper limit of about 0.032 eV. Equation 1 can now be written

$$\frac{dq_c}{dt} = sq_p n \nabla(T) \, \exp[-E(q_c)/kT] \tag{3a}$$

for the case in which there is no incident illumination of sufficient energy to initiate photodesorption and

$$\frac{dq_c}{dt} = sq_p n \bar{v}(T) \, \exp[-E(q_c)/kT] - L \tag{3b}$$

for the case in which photodesorption occurs.

Letting $a'(P,T) = s(T)\nabla(T)q_p(P,T)$ and dropping the subscript c, Equations 3a and 3b become

$$\frac{dq}{dt} = a'(P,T)n \, \exp[-E(q)/kT] \tag{4a}$$

and

38

$$\frac{dq}{dt} = a'(P,T)n \, \exp[-E(q)/kT] - L \qquad (4b)$$

Let the barrier layer have a thickness d and a dielectric permittivity k, and assume a uniform donor density. The barrier layer arises from negative charge held in the surface trapping levels associated with chemisorbed oxygen, the areal density of which is q. If ρ is the positive charge density in the barrier layer, ϕ is potential difference, and x is the coordinate representing the linear distance measured from the surface and positive toward the interior of the solid, the appropriate form of the one-dimensional Poisson equation is

$$\frac{\partial^2 \phi}{\partial x^2} = -\rho/\varkappa \qquad (5)$$

Integrating twice between the limits $x = 0$ and $x = d$ gives $\phi = -\rho d^2/2\varkappa$, which corresponds to a barrier energy height of

$$E(q) = -e\phi = \rho d^2 e/2\varkappa \qquad (6)$$

The negative charge per unit surface area is -eq, so the positive charge per unit volume in the barrier layer is $\rho = eq/d$. Substituting this into Equation 6 gives

$$E(q) = e^2 qd/2\varkappa = e^2 q/C_a \qquad (7)$$

where C_a is the capacitance of the barrier layer per unit area independent of q.

The quantity C_a is a constant if the second initial assumption is fulfilled. Letting $a'(P,T)n = a(P,T)$ and $e^2/C_a kT = b(T)$, the chemisorption rate equations become

$$\frac{dq}{dt} = a \, \exp(-bq) \qquad (8a)$$

and

$$\frac{dq}{d\tau} = a \, \exp(-bq) - L \qquad (8b)$$

39

where t and τ represent two separate time frames.

Using the fourth assumption, these rate equations can now be converted to forms describing the chemisorption-photoconduction process in terms of the time-variable density, $n \equiv n(t)$, of conduction electrons. Let n_s be the value of n for photocurrent saturation, and q_s the corresponding value of q. Consider the general case in which the photocurrent does not reach saturation, but attains a maximum such that the maximum value of n is $n_f = fn_s$, $f \leq 1$. Let q_f be the corresponding value of q. If V is the volume of the solid under consideration and α is the area illuminated, then

$$\Delta N = V\Delta n = V(n_f - n) \text{ and } \Delta Q = \alpha\Delta q = \alpha(q - q_f).$$

It follows from the fourth assumption that

$$q - q_f = V\Delta n/\alpha$$

or

$$q = x_0 \Delta n + q_f \tag{9}$$

where $x_0 = V/\alpha$ is a constant geometrical factor.

Differentiating Equation 9 gives

$$\frac{dq}{dt} = x_0 \frac{d(\Delta n)}{dt}$$

and substitution of the expression for q in Equation 9 into the right side of Equation 8a (the <u>decay</u> equation) gives

$$a \exp(-bq) = a \exp(-bx_0 \Delta n - bq_f).$$

With these changes Equation 8a becomes

$$\frac{d(\Delta n)}{dt} = A \exp(-B\Delta n) \tag{10}$$

where $A = ax_0^{-1}\exp(-bq_f)$ and $B = bx_0$.

But A is a function of n, since $a = a'(P,T)n$. Let $A' = a'(P,T)x_0^{-1}\exp(-bq_f)$. Then

40

$$\frac{d(\Delta n)}{dt} = A'n \exp(-B\Delta n) \tag{11}$$

where $\Delta n \equiv \Delta n(t) = n_f - n(t)$. Let $y = \Delta n/n_f$. Then Equation 11 becomes

$$\frac{dy}{dt} = A'(1 - y)\exp(-\beta y) \tag{12}$$

where $\beta = Bn_f$. Rearranged for integration, Equation 12 becomes

$$\int_0^y \frac{e^{\beta y} dy}{1-y} = \int_0^t A'dt = A't \tag{13}$$

For $y < 1$, $1/(1- y) = 1 + y + y^2 + \ldots$ and $\int_0^y \frac{e^{\beta y} dy}{1-y} =$

$$\int_0^y (1 + y + y^2 + \ldots) \sum_{p=0}^{\infty} \frac{(\beta y)^p}{p!} dy = \frac{1}{\beta} \sum_{p=0}^{\infty} \frac{(\beta y)^{p+1}}{(p+1)!} + \frac{1}{\beta^2} \sum_{p=0}^{\infty} \frac{(\beta y)^{p+2}}{(p+2)p!}$$

plus terms of higher order. Using only the first term of this expansion, Equation 13 becomes

$$A't = \frac{1}{\beta}(e^{\beta y} - 1)$$

or

$$e^{\beta y} = \beta A't + 1 \tag{14}$$

Taking logarithms of both sides and dividing by β gives

$$y = \frac{1}{\beta}\ln(\beta A't + 1) \tag{15}$$

The constant $\beta A'$ has dimensions of reciprocal time, so set $\beta A' = t_d^{-1}$. With this substitution and using $\beta = Bn_f$ and $y = \Delta n/n_f$, Equation 15 reduces to

$$\Delta n = \frac{1}{B} \ln\left(\frac{t}{t_d} + 1\right) \tag{16}$$

where $t_d^{-1} = Bn_f A'$. This expression constitutes a first-order approximation to a solution for Equation 10, and is restricted to cases in which $\Delta n/n_f$ is small. If $\Delta n/n_f$ becomes so large that higher order terms in y can no longer be neglected, then Equation 16 takes the form

$$\Delta n(t) = \frac{1}{B}\ln\left[\frac{t+t_d}{t_d} - \sum_{m=2}^{\infty} \sum_{p=0}^{\infty} \frac{(\beta y)^{p+m}}{\beta^m (p+m)p!}\right] \tag{17}$$

41

in which the summation is positive, since $0 < y < 1$ and $\beta = a^2 n_f x_0 / C_a kT > 0$.

Equation 10, being the rate equation applicable to cases in which there is no desorption due to incident illumination, can be used to describe the photocurrent decay following a period of illumination in which the conduction electron density has reached a maximum value n_f. For cases in which y is small, $\Delta n(t) = n_f - n(t)$ should increase linearly with $\ln(t + t_d)$. However, should the higher order terms represented by the summation in Equation 17 become appreciable, then a plot of $\Delta n(t)$ vs $\ln(t + t_d)$ should be expected to show a sublinear behavior, $\Delta n(t)$ varying as a power of the logarithmic term that is somewhat less than unity.

Now consider the case in which the photodesorption term L enters into the rate equation. The appropriate equation is then

$$\frac{dq}{d\tau} = a \exp(-bq) - L \tag{8b}$$

where illumination begins at time $\tau = 0$. If n_e is the equilibrium conduction electron density in the dark and q_e is the corresponding chemisorbate density, then

$$\alpha(q_e - q) = V(n - n_e) = V\Delta n_e$$

or

$$q = -x_0 \Delta n_e + q_e \tag{18}$$

Note that $\Delta n_e \equiv \Delta n_e(t)$ is not the $\Delta n(t)$ defined for the decay process. Now

$$\frac{dq}{d\tau} = -x_0 \frac{d(\Delta n_e)}{d\tau} \tag{19}$$

and

$$\exp(-bq) = \exp(bx_0 \Delta n_e - bq_e) \tag{20}$$

42

Substituting Equations 19 and 20 into Equation 8b (the _rise_ equation) gives

$$\frac{d(\Delta n_e)}{d\tau} = x_0^{-1}\left[L - A_1\exp(B\Delta n_e)\right] \tag{21}$$

where $B = bx_0$, as before, and $A_1 = a\exp(-bq_e)$. Rewriting and integrating, Equation 21 becomes

$$\int_0^{\Delta n}\frac{d(\Delta n_e)}{L - A_1\exp(B\Delta n_e)} = \int_0^\tau\frac{d\tau}{x_0} = x_0^{-1}\tau \tag{22}$$

or, if the photodesorption rate L is assumed constant,

$$\frac{\Delta n_e}{L} - (BL)^{-1}\left\{\ln[L - A_1\exp(B\Delta n_e)] + \ln(L - A_1)\right\} = \tau/x_0.$$

Rearranging and multiplying by BL, this becomes

$$B\Delta n_e = \ln\left[\frac{L - A_1\exp(B\Delta n_e)}{L - A_1}\right] + BL\tau/x_0.$$

Taking the antilogarithm of both sides and substituting b for B/x_0 gives

$$\exp(B\Delta n_e) = \left[\frac{L - A_1\exp(B\Delta n_e)}{L - A_1}\right]\exp(bL\tau).$$

Regrouping and simplifying, this becomes

$$\exp(B\Delta n_e) = \left[\frac{A_1}{L} + (1 - \frac{A_1}{L})\exp(-bL\tau)\right]^{-1}.$$

Taking logarithms of both sides and dividing by B now gives

$$\Delta n_e(\tau) = -\frac{1}{B}\ln\left[\frac{A_1}{L} + (1 - \frac{A_1}{L})\exp(-bL\tau)\right] \tag{23}$$

This solution, like the solution for the decay equation, is an approximation since A_1 is a function of n. Note that there is no simple relationship between $\Delta n_e(\tau)$ and τ, unless $L \gg A_1$, in which case $\Delta n_e(\tau)$ should approximate a linear function of τ. Also note that if τ becomes very large (photocurrent saturates) Δn_e approaches the constant $(\Delta n_e)_{sat} = B^{-1}\ln(L/A_1)$.

One is to be reminded that the validity of this model for the surface-related photoconductivity of sintered zinc oxide appears

relatively well established and that it has been the purpose of the present report to investigate its applicability to <u>crystals</u> of <u>stannic</u> <u>oxide</u>.